



This is a repository copy of *Investigation on wear and rolling contact fatigue of wheel-rail materials under various wheel/rail hardness ratio and creepage conditions*.

White Rose Research Online URL for this paper:  
<http://eprints.whiterose.ac.uk/154421/>

Version: Accepted Version

---

**Article:**

Hu, Y., Zhou, L., Ding, H.H. et al. (5 more authors) (2020) Investigation on wear and rolling contact fatigue of wheel-rail materials under various wheel/rail hardness ratio and creepage conditions. *Tribology International*, 143. 106091. ISSN 0301-679X

<https://doi.org/10.1016/j.triboint.2019.106091>

---

Article available under the terms of the CC-BY-NC-ND licence  
(<https://creativecommons.org/licenses/by-nc-nd/4.0/>).

**Reuse**

This article is distributed under the terms of the Creative Commons Attribution-NonCommercial-NoDerivs (CC BY-NC-ND) licence. This licence only allows you to download this work and share it with others as long as you credit the authors, but you can't change the article in any way or use it commercially. More information and the full terms of the licence here: <https://creativecommons.org/licenses/>

**Takedown**

If you consider content in White Rose Research Online to be in breach of UK law, please notify us by emailing [eprints@whiterose.ac.uk](mailto:eprints@whiterose.ac.uk) including the URL of the record and the reason for the withdrawal request.

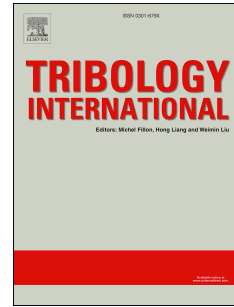


[eprints@whiterose.ac.uk](mailto:eprints@whiterose.ac.uk)  
<https://eprints.whiterose.ac.uk/>

# Journal Pre-proof

Investigation on wear and rolling contact fatigue of wheel-rail materials under various wheel/rail hardness ratio and creepage conditions

Y. Hu, L. Zhou, H.H. Ding, G.X. Tan, R. Lewis, Q.Y. Liu, J. Guo, W.J. Wang



PII: S0301-679X(19)30605-X

DOI: <https://doi.org/10.1016/j.triboint.2019.106091>

Reference: JTRI 106091

To appear in: *Tribology International*

Received Date: 5 August 2019

Revised Date: 26 November 2019

Accepted Date: 26 November 2019

Please cite this article as: Hu Y, Zhou L, Ding HH, Tan GX, Lewis R, Liu QY, Guo J, Wang WJ, Investigation on wear and rolling contact fatigue of wheel-rail materials under various wheel/rail hardness ratio and creepage conditions, *Tribology International* (2019), doi: <https://doi.org/10.1016/j.triboint.2019.106091>.

This is a PDF file of an article that has undergone enhancements after acceptance, such as the addition of a cover page and metadata, and formatting for readability, but it is not yet the definitive version of record. This version will undergo additional copyediting, typesetting and review before it is published in its final form, but we are providing this version to give early visibility of the article. Please note that, during the production process, errors may be discovered which could affect the content, and all legal disclaimers that apply to the journal pertain.

© 2019 Published by Elsevier Ltd.

### **Author Contributions Section**

Y. H. and W.J. W. conceived and designed the experiments. Y. H. and L. Z. performed the sample preparation, carried out the experiments and materials characterization. G.X. T. measured the fatigue crack size and hardness of wheel and rail rollers. R. L., J. G., Q.Y. L. and Y. H. analyzed the results. H.H. D. and Y. H. prepared the manuscript. All authors discussed the experimental results and commented on the manuscript. All authors read and approved the final manuscript.

# Investigation on wear and rolling contact fatigue of wheel-rail materials under various wheel/rail hardness ratio and creepage conditions

Y. Hu<sup>a</sup>, L. Zhou<sup>a</sup>, H.H. Ding<sup>a</sup>, G.X. Tan<sup>b</sup>, R. Lewis<sup>c</sup>, Q.Y. Liu<sup>a</sup>, J. Guo<sup>a</sup>, W.J. Wang<sup>a,\*</sup>

<sup>a</sup> Tribology Research Institute, State Key Laboratory of Traction Power, Southwest Jiaotong University,

Chengdu 610031, China

<sup>b</sup> Business School, Central South University, Changsha, 410083, China

<sup>c</sup> Department of Mechanical Engineering, the University of Sheffield, Mappin Street, Sheffield S1 3JD, UK

**Abstract:** The wear and rolling contact fatigue of wheel-rail materials were investigated through varying wheel/rail hardness ratios ( $H_w/H_r$ ) and creepages. The results indicated that with the  $H_w/H_r$  increasing from 0.927 to 1.218, the wheel wear rate reduced significantly in the case of  $H_w/H_r = 1.218$ , the rail wear rate showed an increasing trend. Both the wheel and rail wear rates increased as the creepage enlarged. The synergistic results of  $H_w/H_r$  and creepage caused a transition of the wear and damage mechanisms on the wheel-rail steels. Besides, the fatigue damage of ER7 and CL60 wheel materials was dominated by slender multi-layer cracks, while the fatigue cracks were short and contained lots of interlayer broken materials on C-class wheel steel.

**Keywords:** Wear rate; Damage mechanism; Synergistic result; Fatigue crack

## 1. Introduction

The wheel-rail interface acts as a vital role in the operating safety and service performance of a railway network. Wear and rolling contact fatigue (RCF) are two common forms of damage, which often exists on the wheel-rail surfaces [1]. The effects of a single

---

\* Corresponding author. Tel: +86-28-87634304.

E-mail address: wwj527@swjtu.cn (W.J. Wang).

factor, such as the operating speed and the axle load, on the wear and RCF characteristics of wheel-rail steels were studied in previous reports [2-4]. The results showed that under the coupling of wear and RCF, the wheel-rail damage of high-speed railway was dominated by RCF, while that of heavy-duty railway was mainly wear. Therefore, the damage mechanism of wheel-rail materials under different operating conditions is different, so different steels should be selected for different working conditions. Besides, investigations [5-7] showed that the rolling direction, spherical dents and the third body (water, oil and sand) had important influences on the crack propagation mechanism and fatigue life of the wheel-rail materials. In practice, the wheel-rail interface is in an open system, it is affected by the synergistic results of multiple factors. Therefore, to optimize the selection of wheel and rail materials in complex service environments and ensure the reliability of the railway, it is necessary to carry out research to study the wear and RCF damage evolution of different wheel-rail steels under multiple parameter conditions.

For a long time, the main wheel-rail materials used in the railway have been lamellar pearlite steels. In order to characterize the matching behavior of different wheel-rail materials, the wheel/rail hardness ratio ( $H_w/H_r$ ) was introduced in previous research [8,9]. As early as 1982, a classical model of the relationship between the hardness ratio and wheel and rail wear loss was proposed by Steele & Reiff [8]. When the  $H_w/H_r > 1$ , with the increase in rail hardness, the wear of the rail steel decreased linearly, while the wear of the wheel steel increased linearly. When the  $H_w/H_r < 1$ , with the increase in rail hardness, the wear of the rail material continued to decrease linearly, while the wear of the wheel material remained stable. Based on this model, the hardness of wheel materials was generally slightly lower than that of

rail materials, i.e.  $H_w/H_r < 1$ . Before the year 2000, researchers tried to increase the rail hardness through heat treatments to reduce its wear loss [9-11]. The results indicated that increasing the rail hardness could reduce the rail wear but increase the wheel wear. However, this conclusion was thought doubtful in recent years. For example, Heyder & Maedler [12] carried out experiments with different standard grades of wheel-rail materials, finding that the R350HT rail with improved hardness reduced both the rail wear and the wheel wear. Contour plots for the relationship between the wear rate and  $H_w/H_r$  were presented by Petrakova et al. through a series small scale tests [13,14], and it was indicated that the optimal  $H_w/H_r$  was 0.91-0.97 or close to 1. Based on these references mentioned, there is still no agreed conclusion about the effect of the change in hardness on the wear of wheel-rail materials. Furthermore, wheel-rail materials with different hardness usually have different microstructures, for example, as the pearlitic lamellar spacing reduces, the hardness of wheel-rail materials increases. The initiation and evolution of wheel-rail RCF is also affected by the material microstructures, as for instance, RCF cracks are primarily initiated at the highly strained ferrite phase and propagated along grain boundaries by cavitation [15,16]. Moreover, varying work hardening levels were found on the pearlitic and bainitic rail materials [17-19]. The work hardening changed the  $H_w/H_r$  during the test, further affecting the wear and RCF behaviours. Thus, carrying out the investigation about the effect of  $H_w/H_r$  on the wear and RCF behaviours of wheel-rail materials is very essential and meaningful.

The creepage is another important factor which has significant effects on the wear and RCF evolution of wheel-rail steels. According to the Archard wear coefficient map [20] and shakedown map [21-23], the rising creepage caused an increasing trend of traction coefficient,

further enhancing the wear rate [24]. As the creepage enlarged, the evolution of wheel-rail wear rates was divided into various regions [25,26]. It was noted that the fatigue damage exacerbated with the rising creepage. For example, the thickness of the plastic deformation layer increased at severe sliding condition [11,26], the serious wheel slipping could result in the rail white etching layer [27], and the growth angle of cracks increased obviously as the creepage enlarged [28]. Meanwhile, when different materials are matched to run with, the evolution of wear and damage behaviours affected by the value of creepage changes a lot [25]. Thus, the investigation on the wear and RCF damage evolution considering both the  $H_w/H_r$  and creepage is the key to the further study.

It is a fact that the hardness and the creepage could influence wear and RCF characteristics of wheel-rail steels. However, under the combined actions of hardness ratios and creepages, the evolution of the wear and damage mechanisms needs to be further clarified. In view of this, the investigation on the wear and fatigue failure evolution of wheel-rail steels under various  $H_w/H_r$  and creepage conditions was carried out. Specifically, the wear transitions mechanism of wheel-rail materials and the growth process of RCF cracks were observed in detail.

## 2. Experimental details

The experiments were performed under dry conditions through a rolling-sliding wear testing apparatus (WR-1, China) [29], as shown in Fig. 1. The apparatus is equipped with upper and lower rollers, i.e., wheel and rail samples. The wheel/rail rollers are driven and controlled by a DC motor (2.0 kW) with a rolling speed from 0 to 1000 rpm. The vertical

force (from 0 to 2000 N) can be applied by adjusting a compressed spring and is measured using a load sensor (LC-7, China, accuracy: 0.1 N). The friction torque and cycles of the lower roller are measured using a torque sensor (TQ-660, China, range:  $0\pm 20$  N·m, accuracy: 0.01 N·m) and revolution sensor, respectively. The creepage of this apparatus can be calculated as following formula.

$$\text{Creepage} = \frac{\omega_{rail}r_{rail} - \omega_{wheel}r_{wheel}}{\omega_{rail}r_{rail}} = \frac{\omega_{rail} - \omega_{wheel}}{\omega_{rail}} \quad (1)$$

Where  $\omega_{rail}$  and  $\omega_{wheel}$  are the rotational speeds of rail and wheel rollers, respectively, and  $r_{rail}$  and  $r_{wheel}$  are the radius of the wheel-rail rollers with same values, respectively. Various creepages (0, 0.17%, 0.91%, 2.38%, 3.83%, 4.55%, 9.43%) can be achieved by altering the relative speeds of the two rollers via selecting and installing the corresponding gear pairs.

The sampling positions of the two rollers and their sizes are presented in Fig. 2. The wheel and rail rollers were cut from the wheel tread and rail head, respectively. The diameter was 40 mm for the wheel-rail rollers, and the contact width between the two rollers was 5 mm. All rollers were polished to a surface roughness (Ra) of approximately 0.15  $\mu\text{m}$ . Before each test, the rollers were thoroughly cleaned by ultrasonic cleaning for 10 min.

Three grades of wheel materials (ER7, CL60, C-class) and one kind of rail steel (U75V) were used in this study. The chemical compositions and hardness are given in Table 1. The ER7 grade wheel is softer than the U75V rail, and the other two wheel steels are harder than the U75V rail. Three wheel/rail hardness ratios ( $H_w/H_r = 0.927, 1.025, \text{ and } 1.218$ ) were achieved by matching the rail roller with different wheel rollers. The microstructures of the wheel and rail materials are presented in Fig. 3. The three wheel materials have ferrite-pearlite microstructure which is composed of netted ferrite and lamellar pearlite (Fig. 3a-c), while the

U75V rail steel has a pearlite microstructure which is composed of lamellae of cementite and ferrite (Fig. 3d). The netted ferrite content of wheel steels decreases with the increasing hardness, especially the C-class wheel with a high hardness of 388 HV<sub>0.5</sub> is almost free of ferrite (Fig. 3c).

All tests were run  $1.8 \times 10^5$  cycles under a rotational speed of 200 r/min, and the contact pressure is set to 850 MPa. The creepages used in this study were 0.17%, 0.91%, 2.38%, 4.55% and 9.43%, respectively. The test parameters are listed in Table 2.

The wear rates (mass loss ( $\mu\text{g}$ ) within a rolling distance of 1 m) of wheel-rail rollers were measured by using an electronic balance (JA4103, accuracy: 0.0001g). The hardness was measured using a Vickers hardness instrument (MVK-H21, Japan). Fig. 4 shows the sampling position of surface and section in the wheel-rail rollers after tests. Three small pieces of 1 mm length were taken from each roller and each piece is separated by 120 degrees. Each section was cut along the rolling direction and mounted in resin, ground with 2000 grit abrasive paper, polished with 0.5  $\mu\text{m}$  diamond and etched with 4% Nital. The surface damage, plastic deformation and fatigue cracks were characterized using optical microscopy (OLYMPUS BX60M, Japan) and scanning electron microscope (SM-6490LV, Japan). The length and depth of each surface crack were measured using OM equipped with an image analysis software (Sisc IAS Professional).

### 3. Results

#### 3.1 Wear rate and hardness

Fig. 5a shows that the adhesion coefficient sharply increases with the creepage rising

from 0.17% to 4.55%, and remains relatively stable under the creepage of 4.55% – 9.43%. Under the creepage of 0.91% and 2.38%, the average adhesion coefficient of in three  $H_w/H_r$  conditions is different (Fig. 5b). This may be due to the difference of the wheel-rail surface damage at the late stage of experiments (about after 30,000 cycles), resulting in different roughness and vibration of the contact interface.

The wheel-rail wear rates changing with creepages are presented in Fig. 6. The experiments under five creepages were performed twice in the case of  $H_w/H_r = 0.927$  while the other experiments were conducted once. When the creepage enlarges from 0.17% to 4.55%, the wheel-rail wear rates in three  $H_w/H_r$  conditions increase rapidly, as shown in Fig. 6. However, under the creepage of 4.55% – 9.43%, there is a slightly drop of wheel wear rate except for the case of  $H_w/H_r = 0.927$ , while the rail wear rates remain fairly stable in the three  $H_w/H_r$  conditions. There is no significant change in wheel wear rate under the three  $H_w/H_r$  conditions at the smallest creepage (0.17%). When the value of creepage is larger than 0.17%, the wheel wear rate in the case of  $H_w/H_r = 1.218$  is significantly lower than the other two  $H_w/H_r$  conditions (Fig. 6a). That is, the wear rate of C-class wheel steel with low ferrite content and a high hardness is significantly lower than the wear rate of ER7 and CL60 wheel materials. Concerning the wear rate of rail material, it presents an obvious ascending trend with the enlargement in the  $H_w/H_r$  (Fig. 6b), i.e., with the increase in the hardness and the decrease in the ferrite content of the matched wheel steels, the rail wear increases significantly.

It should be noted that there might be errors between different experiments due to manufacturing processes, alignment issues and measurement, for example, it might be

possible that the upper and lower rollers are not always perfectly aligned. Therefore, to specifically quantify the wear rate, it is necessary to repeat the experiments to obtain statistical results, which will be carried out in the further work.

The surface hardness of wheel-rail rollers and their hardening ratios are shown in Fig. 7.

The hardening ratio is calculated as following formula.

$$\text{Hardening ratio} = \frac{H_{post} - H_{pre}}{H_{pre}} \quad (2)$$

Where  $H_{post}$  and  $H_{pre}$  are the pre-test and post-test surface hardness, respectively. The pre-test and post-test surface hardness of wheel-rail materials in Fig. 7a and c indicates that the rollers have undergone obvious work hardening during the experiments. Moreover, the post-test surface hardness of three wheel steels is positively correlated with their pre-test hardness (Fig. 7a), while the hardening ratio of various wheel steels has no significant relationship with their pre-test hardness (Fig. 7b). Concerning the rail hardness, the rail hardening ratio at the case of  $H_w/H_r = 1.218$  (matched with C-class wheel) is slightly higher than the other two  $H_w/H_r$  conditions (Fig. 7d).

The variation behaviour of wheel-rail hardness as a function of the depth below the surface is often used to characterize the work hardening and the sub-surface deformation [30,31]. Fig. 8 exhibits that the section hardness gradually drops to the bulk hardness with the increasing distance from surface. The effect of  $H_w/H_r$  on the section hardness of the wheel-rail rollers is related to the creepage. Specifically, at low creepages (2.38%), the section hardness of wheel-rail rollers presents an ascending trend with the  $H_w/H_r$ , while at large creepage conditions (9.43%), the section hardness is nearly unchanged.

### 3.2 Surface damage

SEM images of wheel-rail surface damage under various  $H_w/H_r$  conditions are presented in Fig. 9. The wheel surface damage alleviates with the increase in the initial hardness and the decrease in the ferrite content of wheel steels (i.e., the  $H_w/H_r$  increases), and the damage behaviour transforms from coherent peeling to surface crack. In addition, the surface damage on rail rollers shows the same trend and the damage behaviour transforms from severe adhesion to slight surface cracking. The decrease of the surface damage reduces the roughness after the tests, which causes the adhesion coefficient to decrease with the  $H_w/H_r$  increasing, as exhibited in Fig. 5b.

The wheel surface damage is slight at the lowest creepage (0.17%), which is dominated by small surface cracks and slight peeling (Fig. 10a). When the creepage rises to 0.91% and 2.38%, coherent peeling occurs on the wheel roller surface (Fig. 10b and Fig. 9b). When the creepage further rises to 4.55%, the surface damage, which is mainly caused by spalling, becomes more serious on the wheel surface. It should be noted that coherent peeling appears on the wheel surface and the fatigue alleviates anomalously when the creepage reaches to 9.43%. Concerning the rail rollers, the surface damage is mainly attributed to small surface cracks and slight peeling at the lowest creepage of 0.17%, while it mainly manifests as adhesion as the creepage rises from 0.91% to 9.43%.

The generation of rail surface adhesion is related to the damage characteristics of the matched wheel rollers and the thermal effect which is caused by the increasing creepage [32]. Specifically, in the case of large creepages, the wheel surface damage gets worse. Meanwhile, the flash temperature of the wheel-rail interface enlarges sharply. Under this condition, the debris is mainly formed by thick and small pieces. With the action of the increasing

temperature, the debris tends to adhere on the rail surface. Then, the adhesive wear occurs on the rail surface with the cyclic loading.

### 3.3 Sub-surface damage

OM microscopic observation of cross sections of wheel-rail rollers indicates that the creepage affects the plastic deformation greatly (as shown in Fig. 11). The plastic deformation is slight at the lowest creepage (0.17%), which is attributed to the material flowing parallel to the surface. When the creepage enlarges to 0.91%, the plastic deformation aggravates significantly and the angle of plastic flowing increases sharply.

Fig. 12 presents the SEM images of fatigue cracks at various  $H_w/H_r$  values. The fatigue damage of the wheel-rail rollers are dominated by slender multi-layer cracks and surface cracks when U75V rail steel matches with ER7 and CL60 wheel steels (i.e.,  $H_w/H_r = 0.927$  and 1.025). However, the cracks become short and contain a large number of interlayer broken materials when U75V rail steel matches with C-class wheel steel (i.e.,  $H_w/H_r = 1.218$ ). The difference in the cracks might due to the microstructures of wheel steels. The ER7 and CL60 wheel are hypoeutectoid steel with large amount of netted ferrite (Fig. 3a-b). It is easy for the soft ferrite phase to initiate vacancies because of the low yield limit. The intercrystalline netted ferrite depresses crack growth resistance of the materials strongly. As a result, the cracks grow and propagate along the ferrite flowing structure in the plastic deformation area by cavitation, and it is easier to form the slender multilayer cracks [15,33]. However, the fatigue damage of C-class wheel material is dominated by broken cementite, initiating short cracks with interlayer broken materials among the crack boundaries. It should be noted that the fatigue cracks on U75V rail rollers varies with the matched wheel steels.

This indicates that the rail RCF behaviours is significantly influenced by properties of the counter bodies.

Tables 3-4 present the statistics data from fatigue cracks on wheel-rail rollers. Concerning the cracks on the wheel samples, the average length of cracks is in the range of around 50  $\mu\text{m}$  to 380  $\mu\text{m}$ , the average depth is in the range of around 7.3  $\mu\text{m}$  to 45.9  $\mu\text{m}$ , and the average angle is in the range of around 4.0° to 8.6°. With the increase in creepage, the length and depth of cracks show an ascending trend. With the increase in the  $H_w/H_r$  and the decrease in the netted ferrite content of wheel steels, the length and depth of cracks show a declining trend. Concerning the cracks on the rail samples, the average length of cracks is in the range of around 65  $\mu\text{m}$  to 295  $\mu\text{m}$ , the average depth is in the range of around 8.1  $\mu\text{m}$  to 28.9  $\mu\text{m}$ , and the average angle is in the range of around 2.8° to 11.6°. However, the influences of the creepage and hardness ratio on the depth and length of cracks are not clear.

## 4. Discussion

### 4.1 Evolution of wear and RCF damage

In this study, we systematically explored the effects of both  $H_w/H_r$  and creepage on the wear and RCF evolution of wheel-rail steels through a series of experiments. Three  $H_w/H_r$  conditions (one of which is less than 1, one close to 1, and one greater than 1) were achieved by matching various wheel steels to one rail material. The results showed that the wear rate was related to the material matching behaviour, and the wheel wear rate at the case of  $H_w/H_r = 1.218$  (when the high hardness C-class wheel was matched with the U75V rail) was significantly reduced (Fig. 6a). Besides, the rail wear rate depended on the matched wheel materials and increased significantly with the increasing  $H_w/H_r$  (Fig. 6b). This phenomenon

supports the relationship proposed by Steele & Reiff [8]. Meanwhile, the result is also consistent with other recent wear experimental results for different hardness wheel and rail materials [17,34-37]. For RCF damage, as the hardness of wheel steels and  $H_w/H_r$  increased, both the wheel and rail surface damage alleviated, the fatigue cracks on wheel rollers decreased, and work hardening on rail rollers increased. As the creepage increased, both of the wheel and rail wear rates increased, the RCF damage of wheel-rail rollers, including surface damage, plastic deformation, fatigue cracks, etc., tended to exacerbate. The result supports the effect of creepage on wear and RCF in previous studies [23-28].

From the results above, the wear and fatigue damage underwent a transition with the increasing  $H_w/H_r$  and creepage. As it is known, the wear map, which was widely applied in the wheel-rail wear prediction and numerical simulation, is an effective way to distinguish the wear regimes and transition processes [38-40]. In the present study, the wear maps shown in Fig. 11 are plotted based on  $H_w/H_r$  and slip velocity, where the  $H_w/H_r$  stands for the wheel/rail hardness ratio while the slip velocity presents the velocity difference between the wheel and the rail. According to the value of the wear rate, three regimes, mild wear (the wear rate  $< 50 \mu\text{g/m}$ ), severe wear (the wear rate is between  $50 \mu\text{g/m}$  to  $100 \mu\text{g/m}$ ) and catastrophic wear (the wear rate  $> 100 \mu\text{g/m}$ ), are identified in the wheel wear map (Fig. 13a). Similarly, the mild wear and severe wear are included in the rail wear map (Fig. 13b). The wear rates are fairly small without any obvious change with the  $H_w/H_r$  and slip velocity (i.e., creepage) in the mild wear regime. However, in the other two wear regimes, the wear rates are large and exhibit rapid changes with increases in the  $H_w/H_r$  and slip velocity.

Next, we further explored the damage behaviours occurred on the wheel-rail surface. The

damage mechanism maps based on the surface damage characteristics are exhibited in Fig. 14. Notably, the wear mechanism differs in various regimes on the wear maps. The wheel damage mechanism map (Fig. 14a) presents an extremely similar transition boundary with the wear map (Fig. 13a). Specifically, the wheel damage mechanism map (Fig. 14a) can also be classified into three regions. When the wear is mild, the surface damage behaviours are dominated by mild peeling and surface cracks, indicating that the wear mechanism in this regime is attributed to slight fatigue wear. When the wear changes to become severe, the surface damage behaviours turn to be serious and mainly manifested as coherent peeling. Thus, the wear mechanism in this regime ranges to fatigue wear. When the wear further aggravates, with the surface damage becoming more serious (dominated by severe spalling), the wear of wheel material transforms into severe fatigue wear.

According to the surface damage on rail rollers, the damage mechanism map of rail material (Fig. 14b) is divided into two regions, one of which is dominated by mild peeling and surface fatigue crack, while another is dominated by spalling and adhesion. Meanwhile, the wear mechanism achieves a transition from fatigue wear to the combination of fatigue and adhesion wear as the  $H_w/H_r$  declines and the slip velocity rises (i.e., the creepage increasing).

#### **4.2 Crack growth mechanisms**

According to SEM observation and analysis of fatigue cracks under various  $H_w/H_r$  and creepage conditions, we can see that the creepage exhibits a great influence on crack growth. The fatigue cracks exacerbate with the enlargement in creepage. It can be contributed to the fact that the rise of creepage would increase the traction coefficient, which can provide a large driving force for crack growth [26,28]. Besides, the fatigue crack morphology is closely

related to the material. Specially, it is dominated by slender multi-layer cracks on ER7 and CL60 wheels, while on C-class wheel steel, the cracks are short and contain a large number of interlayer broken materials. This can be explained by the fact that the generation and growth of fatigue cracks differs in the various microstructures of the three wheel materials, as shown in Figs. 15-16.

The ER7 and CL60 wheel are hypoeutectoid steels with large amount of netted ferrite, and the proeutectoid ferrites also act as grain boundaries, as shown in Fig. 15a. Under cyclic loading, the surface layer of wheel material undergo severe plastic deformation [41]. Meanwhile, the pearlite colonies are severe compressed and broken while the ferrites was stretched to shape flowing lines along the shear stress (Fig. 15b). The ferrite phase is soft and its yield limit is small. Therefore, the dislocation tangles and pile-ups are primarily generated at the highly strained ferrite phase boundaries [42]. With the increase in strain, sub-grains occur at the ferrite phase and the sub-grain boundaries are made up of dislocation tangles. At the same time, cavities are formed inside the strained ferrite because of the movement of dislocations [33,43]. With the further increase in strain, the strain-induced ultrafine grains (UFGs) are formed in ferrite phase [41,44]. Meanwhile, the growth and join of cavities induce the micro-crack. The process of micro-crack initiation is shown in Fig. 15c. Sub-surface cracks are formed with the further growth of micro-cracks. Then, surface cracks occurred as the surface material is removed. Besides, the sub-surface cracks join with surface crack tips gradually, resulting in the long and slender multi-layer cracks (Fig. 15d).

The C-class wheel steel exhibits randomly oriented pearlite microstructure which consists of lamellar cementite and ferrite. Meanwhile, pearlite colonies with different

orientations are separated through grain boundaries. Besides, pearlite grains has little ferrite (Fig. 16a). Similarly, as the deformation increases, the pearlite colonies whose lamellar arrangement is consistent with the shear force are severely compressed, and the lamellar spacing decreases sharply, while the pearlite colonies which is arranged at an angle or perpendicular to the shear force are twisted and broken [45,46], as shown in Fig. 16b. During the plastic deformation, dislocation tangles are easy to occur at grain boundaries, resulting in cavities and further forming micro-cracks (Fig. 16c). Notably, the grain boundaries of such materials are not as obvious and continuous as ferrite phase. Therefore, the surface cracks are easy to fracture, and there are many interlayer materials made up by the broken pearlites inside the cracks, as shown in Fig. 16d.

In general, the cracks propagation of both microstructures is dominated by intergranular. Specially, the fatigue cracks on ER7 and CL60 wheel materials primarily generated at the highly strained ferrite phase boundaries, and then grow and propagate along the ferrite flowing lines by cavitation, resulting in the long and slender multi-layer cracks. However, there is almost no ferrite phase in C-class wheel steel, and the grain boundaries are not obvious and discontinuous, thus short cracks with interlayer broken materials tend to initiate in the sub-surface.

In summary, the  $H_w/H_r$  and creepage can be used as important parameters to study the wear and damage transition mechanism of wheel-rail steels. The present work is the pre-study for establishing a wear map based on  $H_w/H_r$  and  $T\gamma/A$ , proposing a mathematical model for the wear and RCF of high-speed wheel and rail under the action of multiple parameters, and optimizing the selection of wheel and rail materials in complex service environments.

However, the range of  $H_w/H_r$  was too small and the observation of the microstructure evolution was not enough. Therefore, it is necessary to carry out experiments with a series  $H_w/H_r$  conditions and investigate the microstructure evolution of wheel-rail materials using Electron Backscatter Diffraction and transmission electron microscope, etc. in the following study. Besides, errors are inevitable during the experimental due to manufacturing and measurement, therefore, experiments need to be repeated to obtain statistically results.

## 5. Conclusions

1. With the  $H_w/H_r$  increasing from 0.927 to 1.218, the wheel wear rate reduces significantly in the case of  $H_w/H_r = 1.218$ , the rail wear rate shows an increasing trend. Both of the wheel and rail wear rates increase as the value of creepage enhanced.

2. As the  $H_w/H_r$  declines and the creepage rise, the wheel wear mechanism changes from mild peeling and slight fatigue wear finally to severe spalling and severe fatigue wear.

3. As the  $H_w/H_r$  declines and the creepage rise, the RCF damage mechanism of rail material changes from mild peeling and surface fatigue crack to spalling and adhesion, and the wear mechanism achieve a transition from fatigue wear to the combination of fatigue and adhesion wear.

4. The fatigue crack morphology is closely related to the microstructures of materials. Fatigue damage on ER7 and CL60 wheels is dominated by slender multi-layer cracks, while on C-class wheel steel, the cracks are short and contain lots of interlayer broken materials.

## Conflicts of interest

There are no conflicts to declare.

### **Author contributions**

Y. H. and W.J. W. conceived and designed the experiments. Y. H. and L. Z. performed the sample preparation, carried out the experiments and materials characterization. G.X. T. measured the fatigue crack size and hardness of wheel and rail rollers. R. L., J. G., Q.Y. L. and Y. H. analyzed the results. H.H. D. and Y. H. prepared the manuscript. All authors discussed the experimental results and commented on the manuscript. All authors read and approved the final manuscript.

### **Acknowledgements**

The work was supported by National Natural Science Foundation of China (Nos. 51775455, 51975489 and 51805446), Program of China Railways Corporation (No. 2017G011-A), Doctoral Innovation Fund Program of Southwest Jiaotong University (No. D-CX201810) and Cultivation Program for the Excellent Doctoral Dissertation of Southwest Jiaotong University.

### **References**

- [1] Y. Zhu, Y. Yang, X. Mu, W. Wang, Z. Yao, H. Yang, Study on wear and RCF performance of repaired damage railway wheels: assessing laser cladding to repair local defects on wheels, *Wear* 430-431 (2019) 126-136.
- [2] W. Zhong, J.J. Hu, Z.B. Li, Q.Y. Liu, Z.R. Zhou, A study of rolling contact fatigue crack

- growth in U75V and U71Mn rails, *Wear* 271 (2011) 388-392.
- [3] C.G. He, Y.B. Huang, L. Ma, J. Guo, W.J. Wang, Q.Y. Liu, M.H. Zhu, Experimental investigation on the effect of tangential force on wear and rolling contact fatigue behaviors of wheel material, *Tribology International* 92 (2015) 307-316.
- [4] W. Zhong, J.J. Hu, P. Shen, C.Y. Wang, Q.Y. Liu, Experimental investigation between rolling contact fatigue and wear of high-speed and heavy-haul railway and selection of rail material, *Wear* 271 (2011) 2485-2493.
- [5] W.R. Tyfour, J.H. Beynon, The effect of rolling direction reversal on fatigue crack morphology and propagation, *Tribology International* 27 (1994) 273-282.
- [6] X.J. Zhao, J. Guo, Q.Y. Liu, E. Butini, L. Marini, E. Meli, A. Rindi, W.J. Wang, Effect of spherical dents on microstructure evolution and rolling contact fatigue of wheel/rail materials, *Tribology International* 127 (2018) 520-532.
- [7] W.J. Wang, R. Lewis, B. Yang, L.C. Guo, Q.Y. Liu, M.H. Zhu, Wear and damage transitions of wheel and rail materials under various contact conditions, *Wear* 362-363(2016)146–152.–
- [8] R. Steele, R. Reiff, Rail-It's behaviour and relationship to total system wear, Proceedings of 2nd Conference on Heavy Haul. Colorado Springs, USA, 1982.
- [9] M. Benson, Effect of differential hardness on wheel/rail wear: literature survey, BRR Report LR MT 006, 1993.
- [10] D. Markov, Laboratory tests for wear of rail and wheel steels, *Wear* 181-183 (1995) 678-686.

- [11]M. Sato, P.M. Anderson, D.A. Rigney, Rolling-sliding behaviour of rail steels, *Wear* 162-164 (1993) 159-172.
- [12]R. Heyder, K. Maedler, The influence of wheel and rail material on the wear of the respective contact partner, *Proceedings of CM2015 10th International Conference on Contact Mechanics and Wear of Rail/Wheel Systems, Colorado, USA, 30 August-3 September 2015, 2015.*
- [13]A.A. Razhkovskiy, T.G. Bunkova, A.G. Petrakova, O.V. Gateluk, Optimization of hardness ratio in rail-wheel friction pair, *Journal of Friction and Wear* 36(4) (2015) 334-341.
- [14]A.G. Petrakova, Optimization of material hardness of solid-rolled wheel of freight cars, *Wear* 30 (2009) 41-45.
- [15]S. Maya-Johnson, A.J. Ramirez, A. Toro, Fatigue crack growth rate of two pearlitic rail steels, *Eng. Fract. Mech.* 138 (2015) 63-72.
- [16]J.E. Garnham, C.L. Davis, The role of deformed rail microstructure on rolling contact fatigue initiation, *Wear* 265 (2008) 1363-1372.
- [17]R. Stock, R. Pippan, RCF and wear in theory and practice-the influence of rail grade on wear and RCF, *Wear* 271 (2011) 125-133.
- [18]S.R. Lewis, S. Fretwell-Smith, P.S. Goodwin, L. Smith, R. Lewis, M. Aslam, D.I. Fletcher, K. Murray, R. Lambert, Improving rail wear and RCF performance using laser cladding, *Wear* 366-367 (2016) 130-136.
- [19]S. Niederhauser, B. Karlsson, P. Sotkovszki, Microstructural development in the heat-affected zone of a laser-cladded steel, *Wear* 96(4) (2005) 370-376.

- [20]T. Jendel, Prediction of wheel profile wear-methodology and verification, (Licentiate Thesis), Royal Institute of Technology, Stockholm, Sweden, 2000 (TRITA-FKT 2000:49).
- [21]K.L. Johnson, Contact Mechanics, Cambridge University Press, Cambridge, 1985.
- [22]Alan R.S. Ponter, H.F. Chen, M. Ciavarella, G. Specchia, Shakedown analyses for rolling and sliding contact problems, *Int. J. Solids Struct.* 43 (2006) 4201–4219.
- [23]G. Donzella, A. Mazzu, C. Petrogalli, Competition between wear and rolling contact fatigue at the wheel–rail interface: some experimental evidence on rail steel, *Proc. IMechE, Part F: J. Rail Rapid Transit* 223 (2009) 31–34.
- [24]Gordana Vasic', Francis J. Franklin, David I. Fletcher, Influence of partial slip and direction of traction on wear rate in wheel-rail contact, *Wear* 270 (2011) 163-171.
- [25]W.T. Zhu, L.C. Guo, L.B. Shi, Z.B. Cai, Q.L. Li, Q.Y. Liu, W.J. Wang, Wear and damage transitions of two kinds of wheel materials in the rolling-sliding contact, *Wear* 398-399 (2018) 79-89.
- [26]L. Ma, C.G. He, X.J. Zhao, J. Guo, Y. Zhu, W.J. Wang, Q.Y. Liu, X.S. Jin, Study on wear and rolling contact fatigue behaviours of wheel-rail materials under different slip ratio conditions, *Wear* 366-367 (2016) 13-26.
- [27]Sarvesh Pal, William J.T. Daniel, Carlos H.G. Valente, Andrew Wilson, Andrej Atrens, Surface damage on new AS60 rail caused by wheel slip, *Engineering Failure Analysis* 22 (2012) 152–165.
- [28]W.J. Wang, S.R. Lewis, R. Lewis, A. Beagles, C.G. He, Q.Y. Liu, The role of slip ratio in rolling contact fatigue of rail materials under wet conditions, *Wear* 376-377 (2017)

1892-1900.

- [29]L. Ma, L.B. Shi, J. Guo, Q.Y. Liu, W.J. Wang, On the wear and damage characteristics of rail material under low temperature environment condition, *Wear* 394 (2018) 149-158.
- [30]S. Khoddam, A.H. Shamdani, P. Mutton, R. Ravitharan, J.H. Beynon, A. Kapoor, A new test to study the cyclic hardening behaviour of a range of high strength rail materials, *Wear* 313 (2014) 43-52.
- [31]A. Kapoor, F.J. Franklin, S.K. Wong, M. Ishida, Surface roughness and plastic flow in rail wheel contact, *Wear* 253(1-2) (2002) 257-264.
- [32]R. Lewis, U. Olofsson, *Wheel-rail interface handbook*, Elsevier, 2009.
- [33]N.P. Suh, The delamination theory of wear, *Wear* 25(1) (1973) 111-124.
- [34]Jung-won Seo, Seok-jin Kwon, Hyun-kyu Jun, Chan-woo Lee, Effects of Wheel Materials on Wear and Fatigue Damage Behaviors of Wheels/Rails, *Tribology Transactions* (2019) 1-15.
- [35]M. Hiensch, M. Steenbergen, Rolling Contact Fatigue on premium rail grades: Damage function development from field data, *Wear* 394 – 395 (2018) 187-194
- [36]R. Stock, D. Eadie, K. Oldknow, Rail grade selection and friction management: a combined approach for optimising rail-wheel contact, *Ironmaking & Steelmaking* 40 (2013) 108-114.
- [37]R. Lewis, P. Christoforou, W.J. Wang, A. Beagles, M. Burstow, S.R. Lewis, Investigation of the influence of rail hardness on the wear of rail and wheel materials under dry conditions (ICRI Wear Mapping Project), *Wear* 430-431 (2019) 383-392.

- [38]R. Lewis, U. Olofsson, Mapping rail wear regimes and transitions, *Wear* 257 (2004) 721-729.
- [39]R. Lewis, R.S. Dwyer-Joyce, U. Olofsson, J. Pombo, J. Ambrosio, M. Pereira, C. Ariaudo, N. Kuka, Mapping railway wheel material wear mechanisms and transitions, *Proceedings of the Institution of Mechanical Engineers, Part F: Journal of Rail and Rapid Transit* 224 (3) (2010) 125-137.
- [40]H.H. Ding, C.G. He, L. Ma, J. Guo, Q.Y. Liu, W.J. Wang, Wear mapping and transitions in wheel and rail material under different contact pressure and sliding velocity conditions, *Wear* 352-353 (2016) 1-8.
- [41]Y. Hu, C.R. Su, L.C. Guo, Q.Y. Liu, J. Guo, Z.R. Zhou, W.J. Wang, Effect of rolling direction on microstructure evolution of CL60 wheel steel, *Wear* 424-425 (2019) 203-215.
- [42]W. Lojkowski, M. Djahanbakhsh, G. Bürkle, S. Gierlotka, W. Zielinski, H.J. Fecht, Nanostructure formation on the surface of railway tracks, *Materials Science and Engineering: A* 303 (2001) 197-208.
- [43]B. Hwang, S. Lee, Y.C. Kim, N.J. Kim, D.H. Shin, Microstructural development of adiabatic shear bands in ultra-fine-grained low-carbon steels fabricated by equal channel angular pressing, *Materials Science and Engineering: A* 441 (2006) 308-320.
- [44]B. Eghbali, Study on the ferrite grain refinement during intercritical deformation of a microalloyed steel, *Materials Science and Engineering: A* 527(2010) 3407-3410.

- [45]T. Leitner, G. Trummer, R. Pippan, A. Hohenwarter, Influence of severe plastic deformation and specimen orientation on the fatigue crack propagation behaviour of a pearlitic steel, *Materials Science and Engineering: A* 710 (2018) 260-270.
- [46]F. Wetscher, R. Stock, R. Pippan, Changes in the mechanical properties of a pearlitic steel due to large shear deformation, *Materials Science and Engineering: A* 445 (2007) 237-243.

Journal Pre-proof

**Figure caption**

Fig. 1: Scheme of the testing apparatus.

Fig. 2: Sampling position and sizes of wheel-rail rollers.

Fig. 3: The microstructures of the wheel-rail materials, (a) ER7 wheel; (b) CL60 wheel; (c) C-class wheel; (d) U75V rail.

Fig. 4: Sampling position of surface and section in the wheel-rail rollers after tests.

Fig. 5: Adhesion coefficient, (a) as a function of cycles ( $H_w/H_r = 1.025$ ); (b) as a function of creepage.

Fig. 6: Wear rate changing with the  $H_w/H_r$  and creepage, (a) wheel; (b) rail.

Fig. 7: Surface hardness and hardening ratio (which is defined by the ratio of increasing hardness to initial hardness), (a) wheel surface hardness; (b) wheel hardening ratio; (c) rail surface hardness; (d) rail hardening ratio.

Fig. 8: Section hardness under different hardness ratios, (a) wheel; (b) rail.

Fig. 9: SEM micrographs of surface damage of wheel-rail rollers under different hardness ratios (creepage = 2.38%), (a)  $H_w/H_r = 0.927$ ; (b)  $H_w/H_r = 1.025$ ; (c)  $H_w/H_r = 1.218$ .

Fig. 10: SEM micrographs of surface damage of wheel-rail rollers under different creepage conditions ( $H_w/H_r = 1.025$ ), (a) 0.17%; (b) 0.91%; (c) 4.55%; (d) 9.43%.

Fig. 11: OM micrographs of plastic deformation of wheel-rail rollers under different creepage conditions ( $H_w/H_r = 1.025$ ), (a) 0.17%; (b) 0.91%.

Fig. 12: SEM micrographs of fatigue cracks on wheel-rail rollers under different  $H_w/H_r$  conditions (creepage = 2.38%), (a)  $H_w/H_r = 0.927$ ; (b)  $H_w/H_r = 1.025$ ; (c)  $H_w/H_r = 1.218$ .

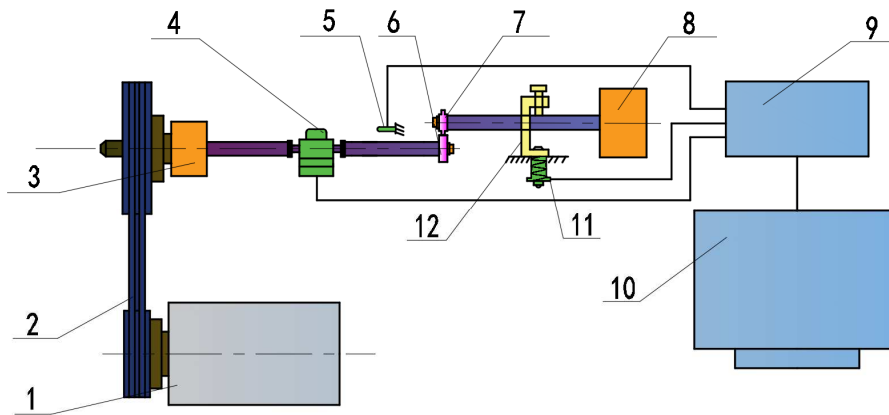
Fig. 13: Wear maps, (a) wheel; (b) rail.

Fig. 14: Damage mechanism maps, (a) wheel; (b) rail.

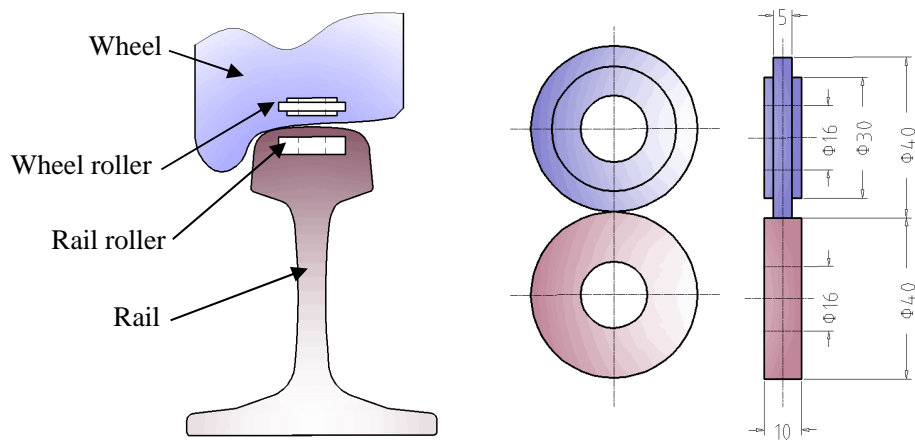
Fig. 15: Schematic illustration of the fatigue crack growth on ER7 wheel material.

Fig. 16: Schematic illustration of the fatigue crack growth on C-class wheel material.

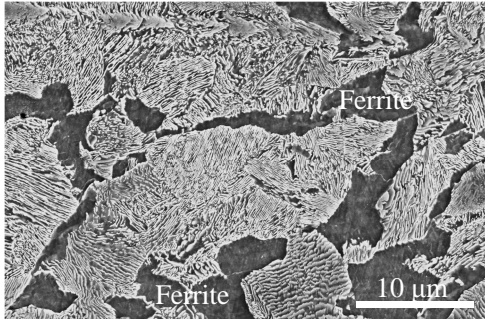
Journal Pre-proof

**Fig. 1: Scheme of the testing apparatus.**

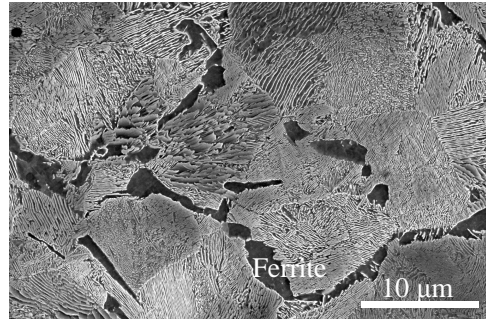
1-DC motor; 2-Drive belt; 3, 8- Gear set; 4-Torque sensor; 5-Revolution sensor; 6-Lower roller; 7-Upper roller; 9-Controller; 10-Computer; 11-Load sensor; 12-Compressed spring.

**Fig. 2: Sampling position and sizes of wheel-rail rollers.**

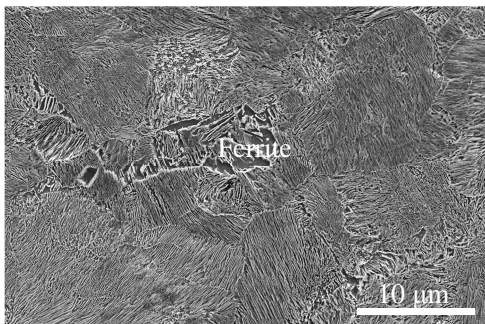
**Fig. 3: The microstructures of the wheel-rail materials, (a) ER7 wheel; (b) CL60 wheel; (c) C-class wheel; (d) U75V rail.**



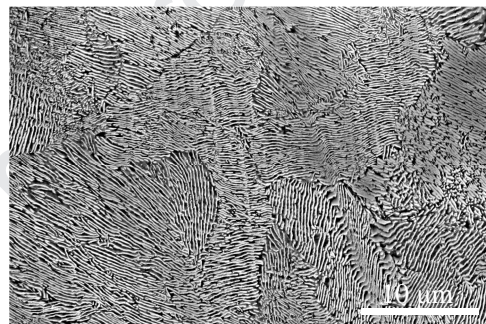
(a)



(b)



(c)



(d)

**Fig. 4: Sampling position of surface and section in the wheel-rail rollers after tests.**

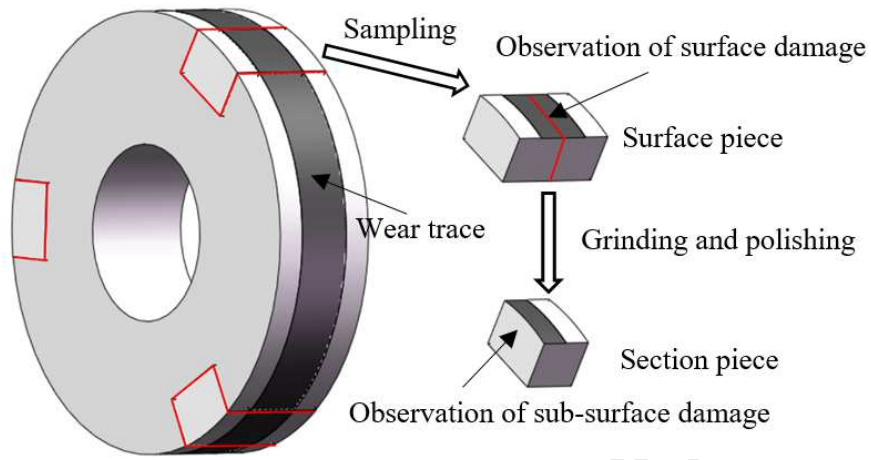


**Fig. 5: Adhesion coefficient, (a) as a function of cycles ( $H_w/H_r = 1.025$ ); (b) as a function of creepage.**

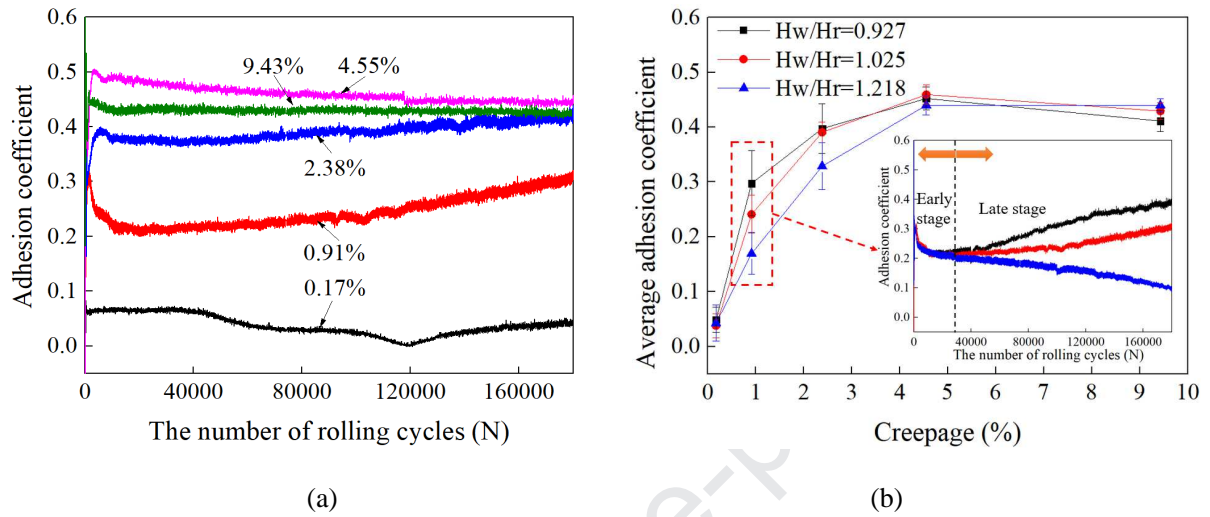


**Fig. 6:** Wear rate changing with the  $H_w/H_r$  and creepage, (a) wheel; (b) rail.

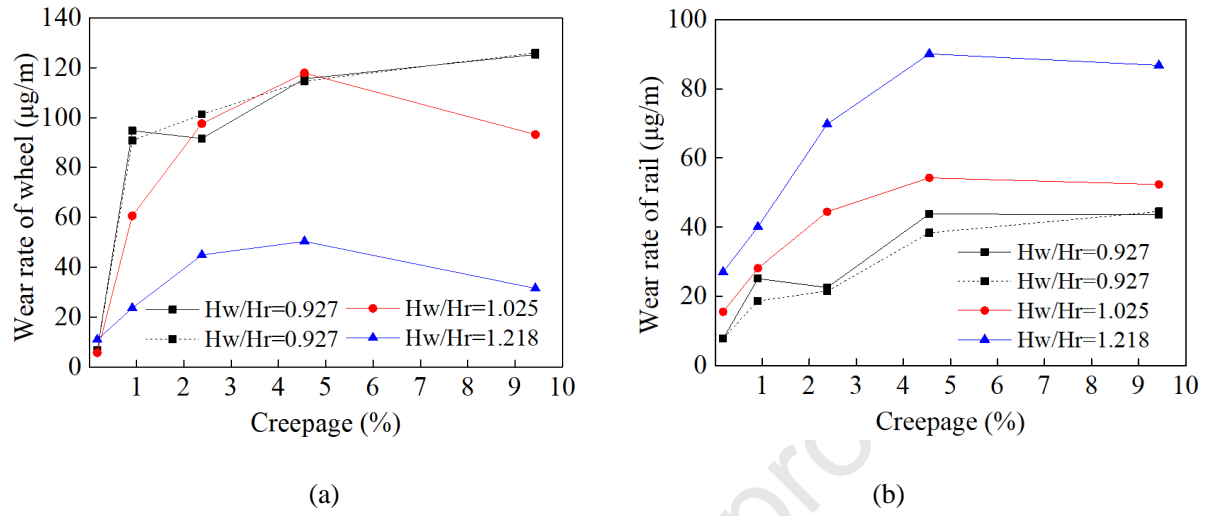
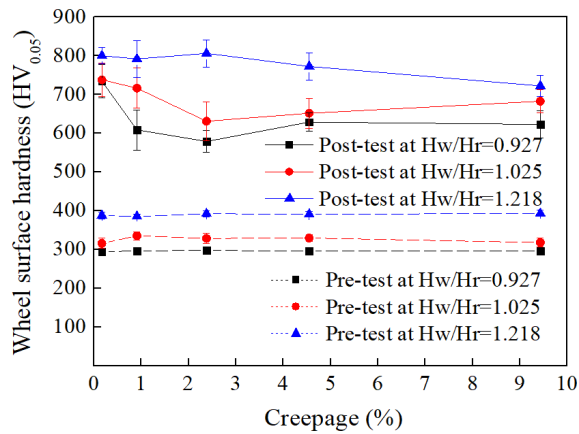
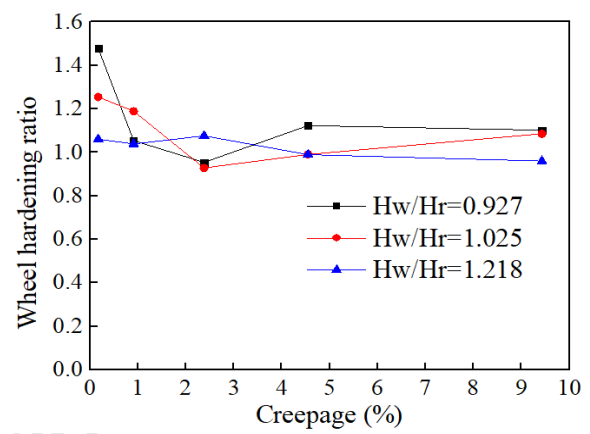


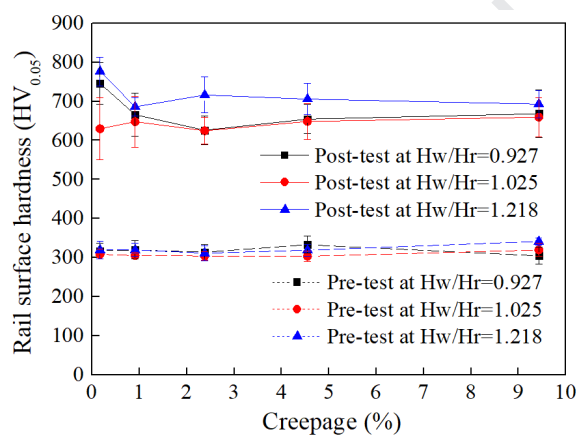
**Fig. 7: Surface hardness and hardening ratio (which is defined by the ratio of increasing hardness to initial hardness), (a) wheel surface hardness; (b) wheel hardening ratio; (c) rail surface hardness; (d) rail hardening ratio.**



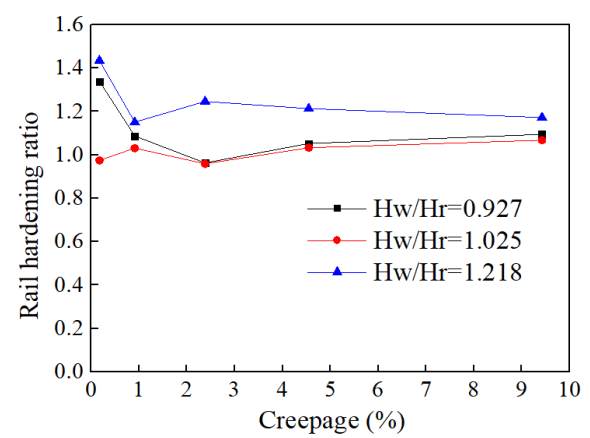
(a)



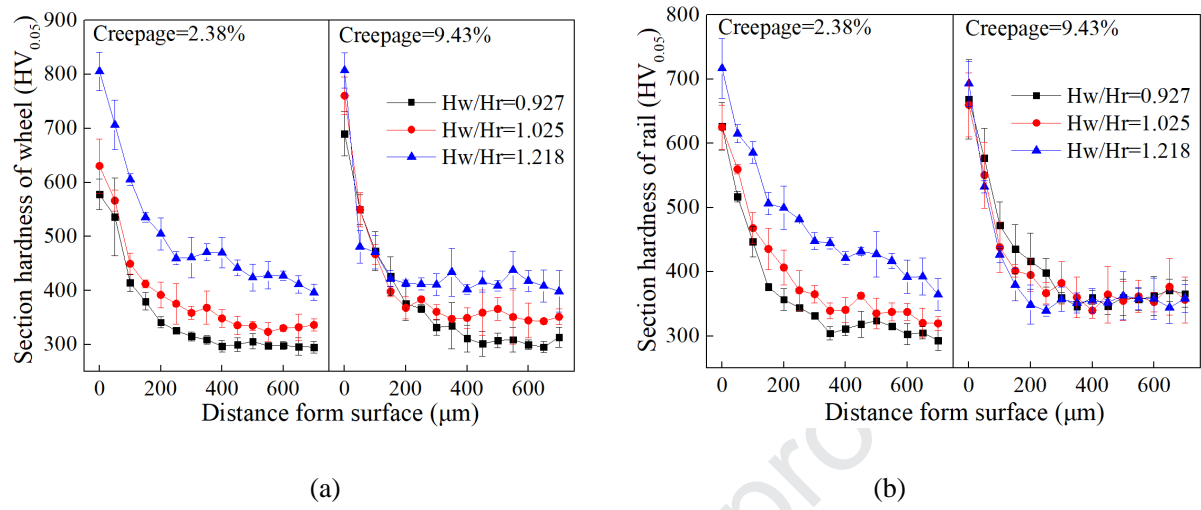
(b)



(c)



(d)

**Fig. 8: Section hardness under different hardness ratios, (a) wheel; (b) rail.**

**Fig. 9: SEM micrographs of surface damage of wheel-rail rollers under different hardness ratios (creepage = 2.38%), (a)  $H_w/H_r = 0.927$ ; (b)  $H_w/H_r = 1.025$ ; (c)  $H_w/H_r = 1.218$ .**

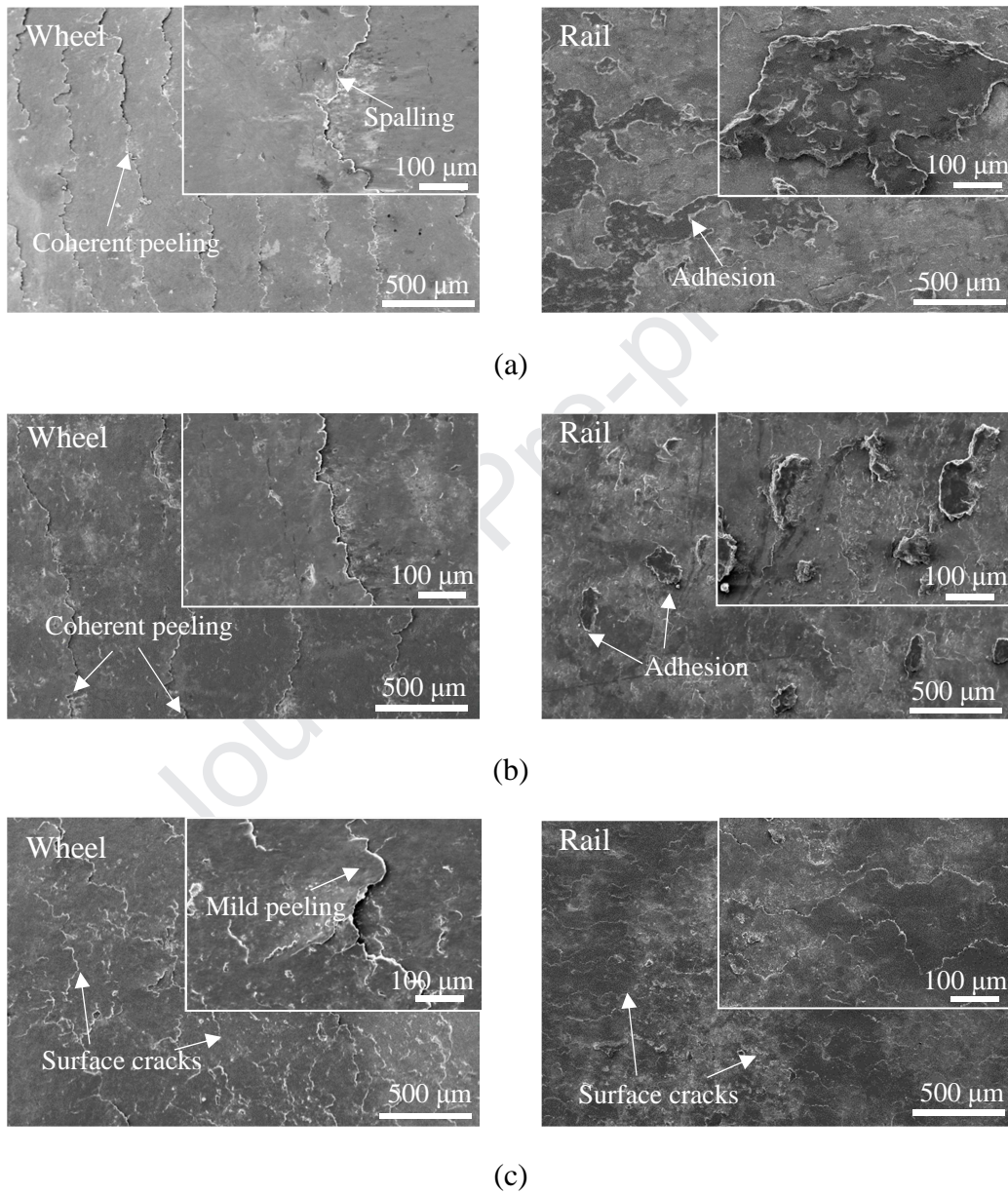
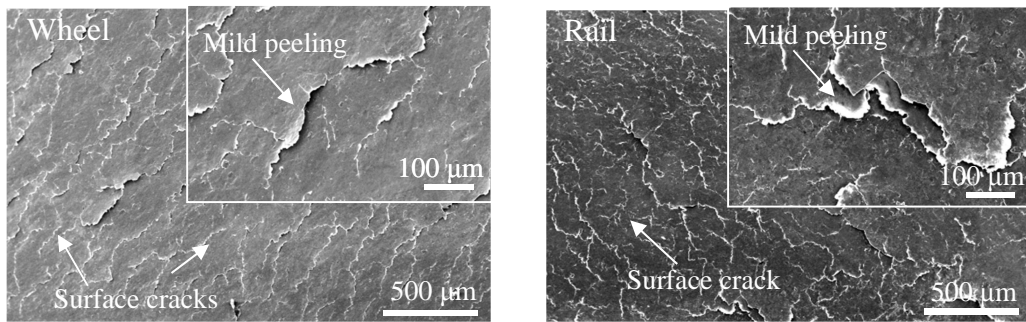
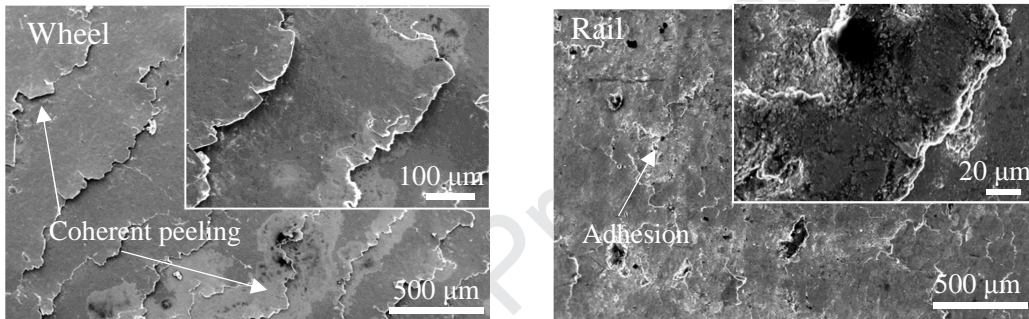


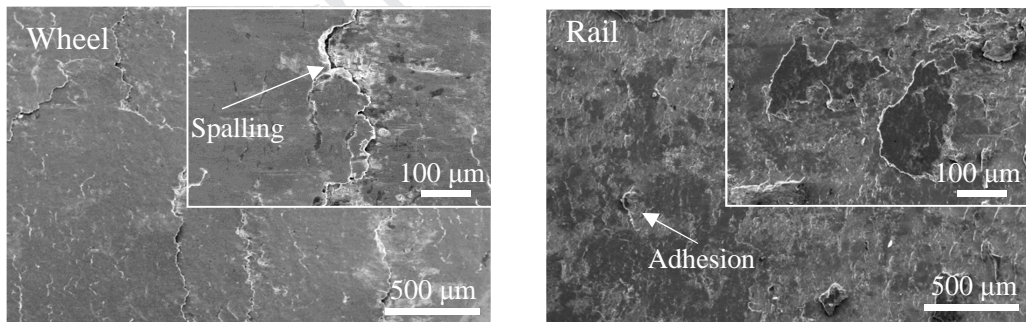
**Fig. 10: SEM micrographs of surface damage of wheel-rail rollers under different creepage conditions ( $H_w/H_r = 1.025$ ), (a) 0.17%; (b) 0.91%; (c) 4.55%; (d) 9.43%.**



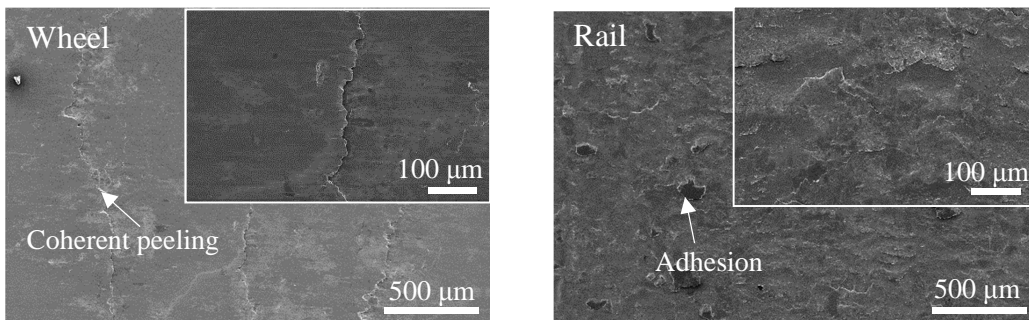
(a)



(b)

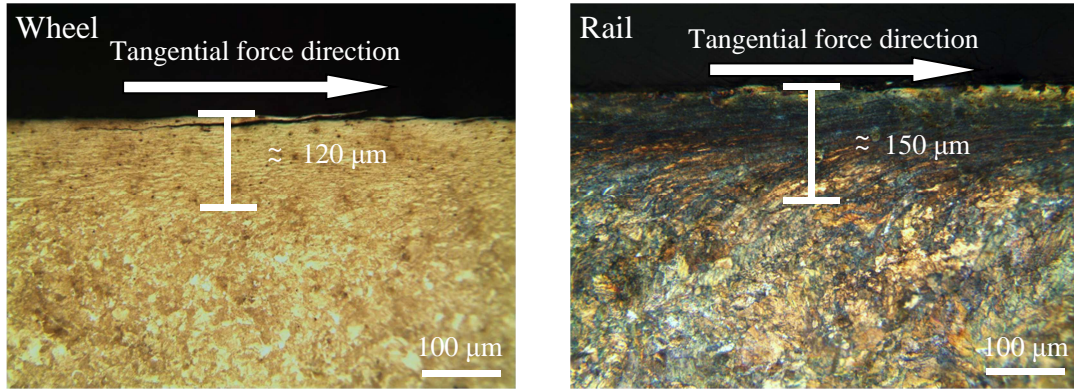


(c)

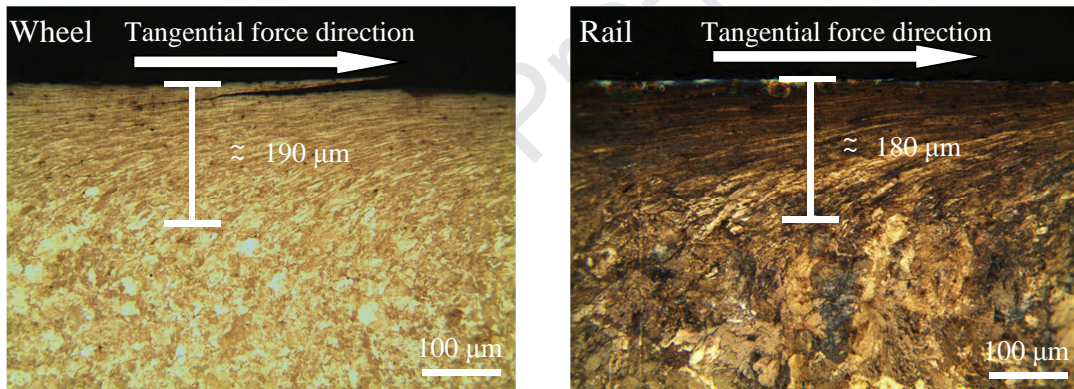


(d)

**Fig. 11: OM micrographs of plastic deformation of wheel-rail rollers under different creepage conditions ( $H_w/H_r = 1.025$ ), (a) 0.17%; (b) 0.91%.**



(a)



(b)

**Fig. 12: SEM micrographs of fatigue cracks on wheel-rail rollers under different  $H_w/H_r$  conditions (creepage = 2.38%), (a)  $H_w/H_r = 0.927$ ; (b)  $H_w/H_r = 1.025$ ; (c)  $H_w/H_r = 1.218$ .**

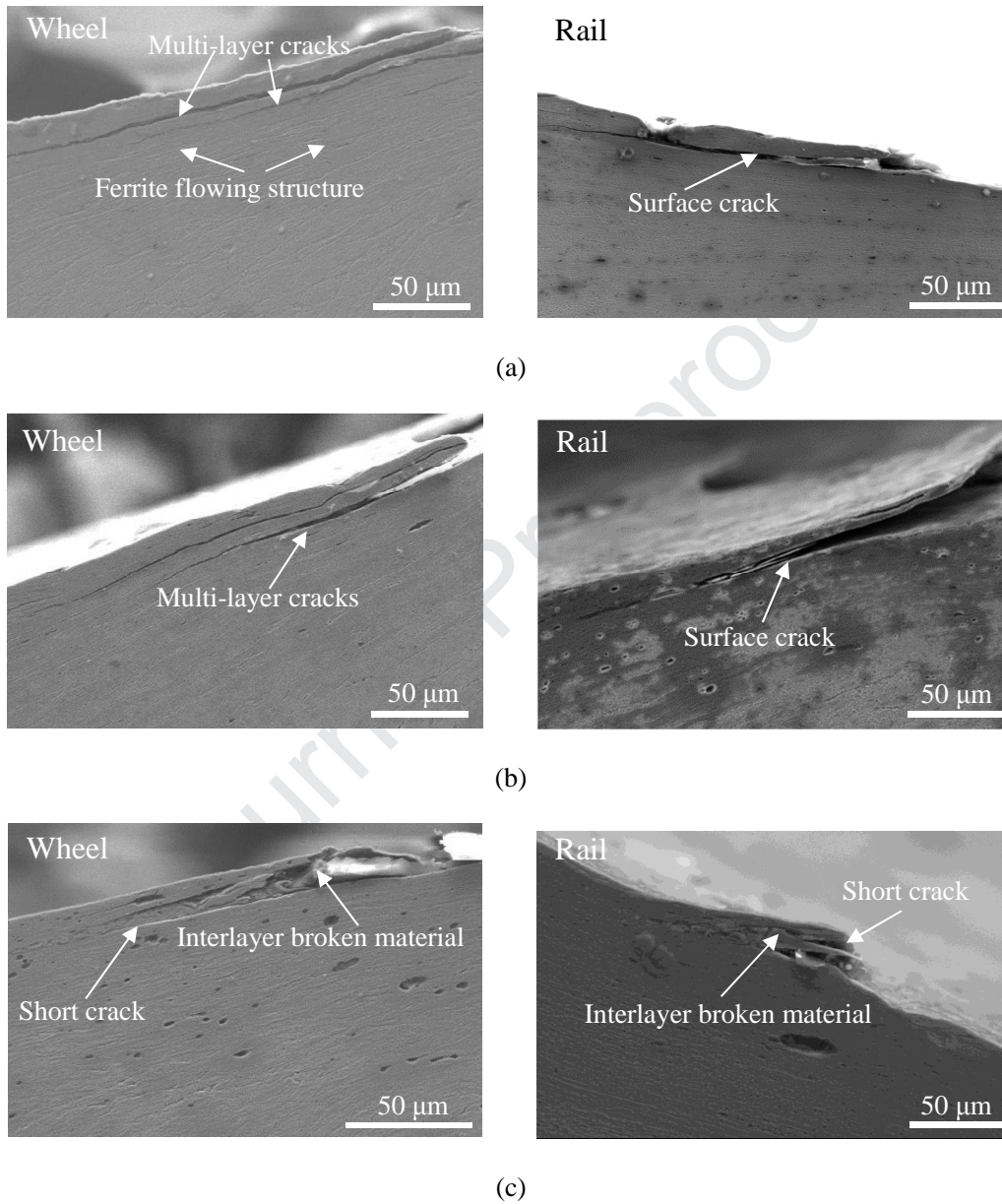
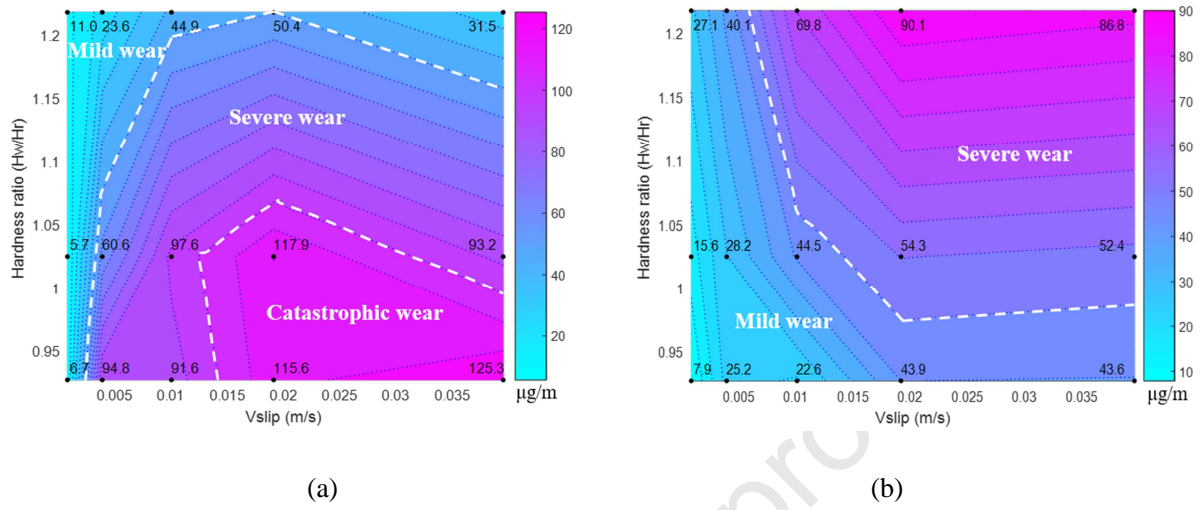
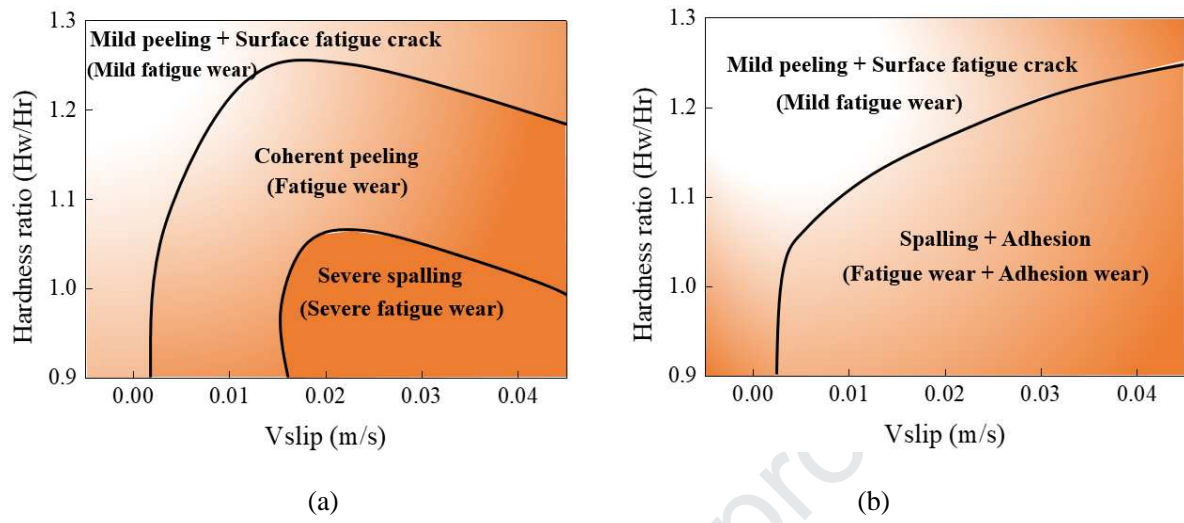
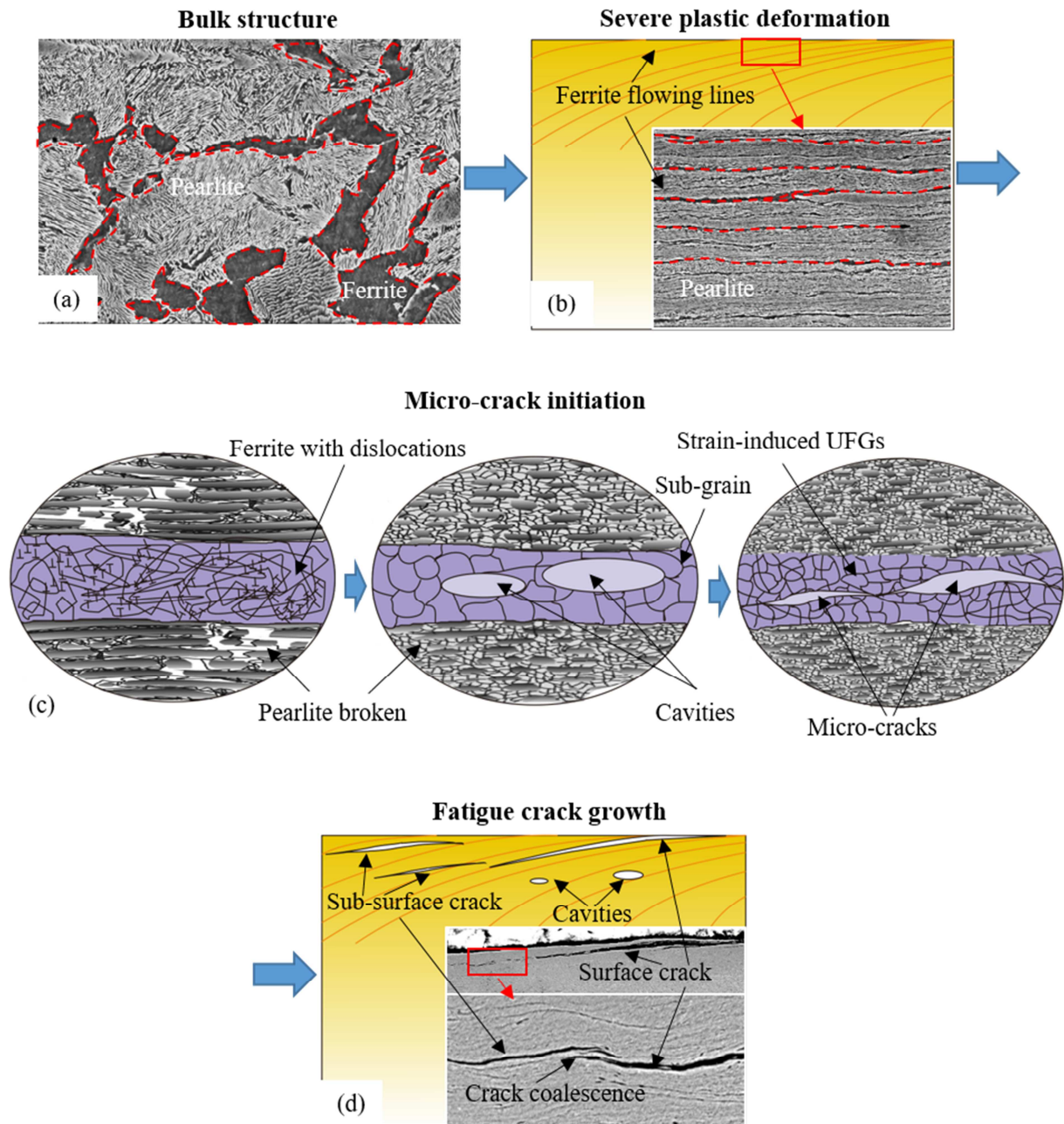


Fig. 13: Wear maps, (a) wheel; (b) rail.



**Fig. 14: Damage mechanism maps, (a) wheel; (b) rail.**

**Fig. 15: Schematic illustration of the fatigue crack growth on ER7 wheel material.**



**Fig. 16: Schematic illustration of the fatigue crack growth on C-class wheel material.**

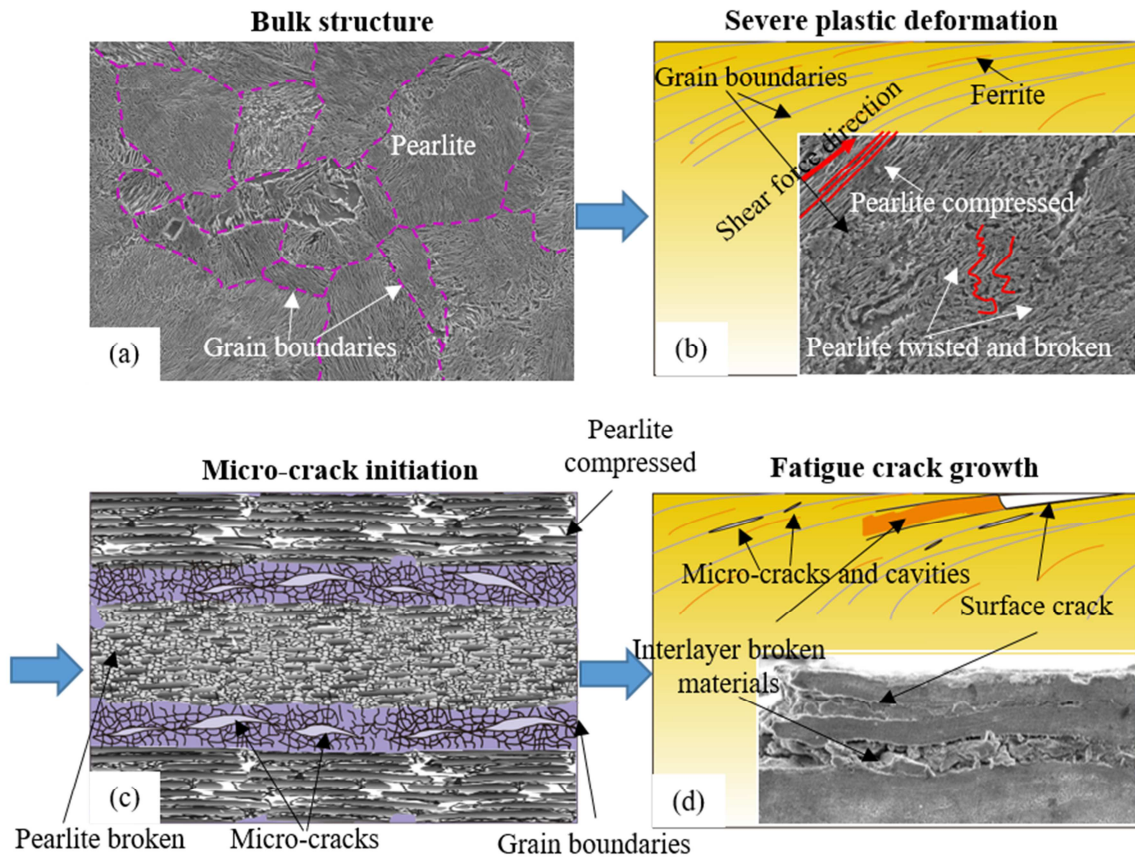


**Table caption**

Table 1: Chemical compositions and hardness of wheel-rail rollers.

Table 2: Summary of test parameters.

Table 3: The size statistics of fatigue cracks on wheel rollers.

Table 4: The size statistics of fatigue cracks of rail rollers.

Journal Pre-proof

**Table 1: Chemical compositions and hardness of wheel-rail rollers.**

| Component | Grade   | Chemical composition (wt%) |           |           |        |             | Hardness/HV <sub>0.5</sub> |
|-----------|---------|----------------------------|-----------|-----------|--------|-------------|----------------------------|
|           |         | C                          | Si        | Mn        | P      | S           |                            |
| Wheel     | ER7     | ≤0.48                      | ≤0.40     | ≤0.75     | 0.020  | 0.015       | 296±6                      |
|           | CL60    | 0.55-0.65                  | 0.17-0.37 | 0.50-0.80 | 0.035  | 0.040       | 327±11                     |
|           | C-class | 0.67-0.77                  | 0.15-1.00 | 0.60-0.90 | 0.030  | 0.005-0.040 | 388±9                      |
| Rail      | U75V    | 0.65-0.75                  | 0.15-0.58 | 0.70-1.20 | ≤0.025 | ≤0.025      | 319±15                     |

**Table 2: Summary of test parameters.**

| Test number | Wheel grade | Rail grade | Hardness ratio/(Hw/Hr) | Creepage/% | Test speed/(r/min) | Maximum contact pressure/MPa | Total number of cycles/N |
|-------------|-------------|------------|------------------------|------------|--------------------|------------------------------|--------------------------|
| 1           | ER7         | U75V       | 0.927                  | 0.17       | 200                | 850                          | 180,000                  |
| 2           | ER7         | U75V       | 0.927                  | 0.91       | 200                | 850                          | 180,000                  |
| 3           | ER7         | U75V       | 0.927                  | 2.38       | 200                | 850                          | 180,000                  |
| 4           | ER7         | U75V       | 0.927                  | 4.55       | 200                | 850                          | 180,000                  |
| 5           | ER7         | U75V       | 0.927                  | 9.43       | 200                | 850                          | 180,000                  |
| 6           | CL60        | U75V       | 1.025                  | 0.17       | 200                | 850                          | 180,000                  |
| 7           | CL60        | U75V       | 1.025                  | 0.91       | 200                | 850                          | 180,000                  |
| 8           | CL60        | U75V       | 1.025                  | 2.38       | 200                | 850                          | 180,000                  |
| 9           | CL60        | U75V       | 1.025                  | 4.55       | 200                | 850                          | 180,000                  |
| 10          | CL60        | U75V       | 1.025                  | 9.43       | 200                | 850                          | 180,000                  |
| 11          | C-class     | U75V       | 1.218                  | 0.17       | 200                | 850                          | 180,000                  |
| 12          | C-class     | U75V       | 1.218                  | 0.91       | 200                | 850                          | 180,000                  |
| 13          | C-class     | U75V       | 1.218                  | 2.38       | 200                | 850                          | 180,000                  |
| 14          | C-class     | U75V       | 1.218                  | 4.55       | 200                | 850                          | 180,000                  |
| 15          | C-class     | U75V       | 1.218                  | 9.43       | 200                | 850                          | 180,000                  |

**Table 3: The size statistics of fatigue cracks on wheel rollers.**

| Creepage (%) | Hw/Hr=0.927                      |                                 |                      | Hw/Hr=1.025                      |                                 |                      | Hw/Hr=1.218                      |                                 |                      |
|--------------|----------------------------------|---------------------------------|----------------------|----------------------------------|---------------------------------|----------------------|----------------------------------|---------------------------------|----------------------|
|              | Average length ( $\mu\text{m}$ ) | Average depth ( $\mu\text{m}$ ) | Average angle (Deg.) | Average length ( $\mu\text{m}$ ) | Average depth ( $\mu\text{m}$ ) | Average angle (Deg.) | Average length ( $\mu\text{m}$ ) | Average depth ( $\mu\text{m}$ ) | Average angle (Deg.) |
| 0.17         | 126 $\pm$ 45                     | 9.7 $\pm$ 3.3                   | 4.4 $\pm$ 1.3        | 125 $\pm$ 72                     | 7.3 $\pm$ 2.9                   | 4.0 $\pm$ 2.3        | 50 $\pm$ 15                      | 7.5 $\pm$ 1.9                   | 8.6 $\pm$ 2.5        |
| 0.91         | 333 $\pm$ 98                     | 32.5 $\pm$ 13                   | 5.2 $\pm$ 2.1        | 207 $\pm$ 101                    | 15.5 $\pm$ 5.6                  | 4.3 $\pm$ 1.3        | 71 $\pm$ 32                      | 7.7 $\pm$ 3.8                   | 6.9 $\pm$ 2.3        |
| 2.38         | 298 $\pm$ 68                     | 28.6 $\pm$ 6.8                  | 5.6 $\pm$ 1.1        | 175 $\pm$ 57                     | 17.5 $\pm$ 7.7                  | 5.7 $\pm$ 1.7        | 160 $\pm$ 59                     | 20.1 $\pm$ 5.3                  | 7.6 $\pm$ 1.9        |
| 4.55         | 214 $\pm$ 75                     | 23.2 $\pm$ 7.6                  | 6.5 $\pm$ 1.4        | 258 $\pm$ 69                     | 32.5 $\pm$ 10                   | 7.3 $\pm$ 1.3        | 152 $\pm$ 35                     | 18.8 $\pm$ 6.0                  | 7.3 $\pm$ 2.5        |
| 9.43         | 380 $\pm$ 116                    | 45.9 $\pm$ 7.7                  | 7.2 $\pm$ 1.2        | 174 $\pm$ 67                     | 22.8 $\pm$ 11                   | 7.6 $\pm$ 2.8        | 156 $\pm$ 30                     | 21.9 $\pm$ 3.1                  | 8.2 $\pm$ 1.3        |

**Table 4: The size statistics of fatigue cracks of rail rollers.**

| Creepage (%) | Hw/Hr=0.927                      |                                 |                      | Hw/Hr=1.025                      |                                 |                      | Hw/Hr=1.218                      |                                 |                      |
|--------------|----------------------------------|---------------------------------|----------------------|----------------------------------|---------------------------------|----------------------|----------------------------------|---------------------------------|----------------------|
|              | Average length ( $\mu\text{m}$ ) | Average depth ( $\mu\text{m}$ ) | Average angle (Deg.) | Average length ( $\mu\text{m}$ ) | Average depth ( $\mu\text{m}$ ) | Average angle (Deg.) | Average length ( $\mu\text{m}$ ) | Average depth ( $\mu\text{m}$ ) | Average angle (Deg.) |
| 0.17         | 275 $\pm$ 65                     | 26.4 $\pm$ 9.5                  | 5.5 $\pm$ 1.7        | 295 $\pm$ 82                     | 25.7 $\pm$ 5.1                  | 5.0 $\pm$ 1.4        | 160 $\pm$ 35                     | 13.1 $\pm$ 3.8                  | 4.7 $\pm$ 1.6        |
| 0.91         | 293 $\pm$ 78                     | 24.5 $\pm$ 6.3                  | 4.8 $\pm$ 1.5        | 284 $\pm$ 62                     | 20.8 $\pm$ 4.9                  | 4.2 $\pm$ 1.2        | 199 $\pm$ 42                     | 9.7 $\pm$ 2.6                   | 2.8 $\pm$ 1.1        |
| 2.38         | 226 $\pm$ 48                     | 14.6 $\pm$ 4.8                  | 3.7 $\pm$ 1.1        | 199 $\pm$ 57                     | 9.7 $\pm$ 3.3                   | 2.8 $\pm$ 1.4        | 65 $\pm$ 21                      | 8.1 $\pm$ 4.8                   | 8.2 $\pm$ 6.0        |
| 4.55         | 209 $\pm$ 45                     | 10.2 $\pm$ 4.2                  | 2.8 $\pm$ 1.2        | 167 $\pm$ 78                     | 16.4 $\pm$ 10                   | 5.5 $\pm$ 1.9        | 89 $\pm$ 39                      | 16.9 $\pm$ 5.3                  | 11.6 $\pm$ 2.7       |
| 9.43         | 181 $\pm$ 78                     | 28.6 $\pm$ 11                   | 9.2 $\pm$ 1.9        | 151 $\pm$ 56                     | 18.4 $\pm$ 8.4                  | 7.2 $\pm$ 2.5        | 190 $\pm$ 82                     | 28.9 $\pm$ 21                   | 8.2 $\pm$ 2.8        |

### Highlights

1. As  $H_w/H_r$  increases, the wheel wear rate declines while the rail wear rate increases.
2. With the slip ratio increasing, both of the wheel and rail wear rates increase.
3. The wear and fatigue damage mechanisms transform as the  $H_w/H_r$  and slip ratio increase.
4. The fatigue crack morphology is closely related to the microstructures of materials.

### **Declaration of Interest Statement**

This paper has not been published previously, that it is not under consideration for publication elsewhere. We declare that we have no conflict of interest.

Journal Pre-proof